ACS APPLIED MATERIALS & INTERFACES

Research Article

www.acsami.org

Facile Fabrication of Poly(L-lactic Acid)-Grafted Hydroxyapatite/Poly(lactic-*co*-glycolic Acid) Scaffolds by Pickering High Internal Phase Emulsion Templates

Yang Hu, Xiaoyu Gu, Yu Yang, Jian Huang, Meng Hu, Weike Chen, Zhen Tong, and Chaoyang Wang*

Research Institute of Materials Science, South China University of Technology, Guangzhou 510640, People's Republic of China

Supporting Information

ABSTRACT: Porous scaffolds consisting of bioactive inorganic nanoparticles and biodegradable polymers have gained much interest in bone tissue engineering. We report here a facile approach to fabricating poly(L-lactic acid)-grafted hydroxyapatite (g-HAp)/poly(lactide-*co*-glycolide) (PLGA) nanocomposite (NC) porous scaffolds by solvent evaporation of Pickering high internal phase emulsion (HIPE) templates, where g-HAp nanoparticles act as particulate stabilizers. The resultant porous scaffolds exhibit an open and rough pore structure. The pore structure and mechanical properties of the scaffolds can be tuned readily by varying the g-HAp nanoparticle concentration and internal phase volume fraction of the emulsion templates. With increasing the g-HAp concentration or decreasing the internal phase volume fraction, the pore size and the porosity decrease, while the Young's modulus and the compressive stress enhance. Moreover, the in vitro mineralization tests show that the bioactivity of the scaffolds increases with increasing the g-HAp concentration. Furthermore, the anti-inflammatory drug ibuprofen (IBU) is loaded into the scaffolds, and the drug release studies indicate that the loaded-IBU exhibits a sustained release profile. Finally, in vitro cell culture assays prove that the scaffolds are biocompatible because of supporting adhesion, spreading, and proliferation of mouse bone mesenchymal stem cells. All the results indicate that the solvent evaporation based on Pickering HIPE templates is a promising alternative method to fabricate NC porous scaffolds for potential bone tissue engineering applications.

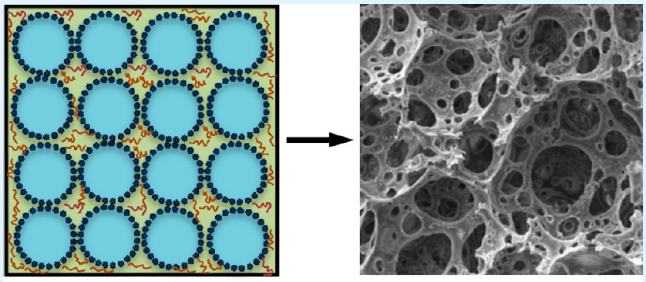

KEYWORDS: *Pickering high internal phase emulsions, poly(lactide-co-glycotide), hydroxyapatite, porous scaffold, solvent evaporation*

1. INTRODUCTION

The bone tissue engineering approach holds great promise in providing an improved clinical therapy to repair damaged and diseased bones.[1,2] In this approach, one of the main goals is to fabricate suitable engineering scaffolds for bone graft substitutes.[3] These scaffolds can not only mimic the biochemical and physical environment of native bone extracellular matrix, but also serve as a temporary three-dimensional template for cell attachment, proliferation, differentiation, and the subsequent bone regeneration.[4−6] To achieve this goal, the ideal scaffolds for bone tissue engineering application should meet certain criteria, including good biocompatibility, excellent bioactivity, adequate mechanical property to resist physiological loads during healing, and appropriate biodegradability at a rate commensurate with remodeling.[7,8] Additionally, it is noted that implantation of engineered scaffolds might result in local inflammation response.[9,10] In this aspect, adding an anti-inflammatory drug into engineered scaffolds can attenuate the local inflammatory response. Thus, the engineering scaffolds should also possess the controlled drug release properties to achieve the long-term anti-inflammatory efficacy and low side effect.

Synthetic biodegradable polyesters, especially poly(L-lactic acid) (PLLA) and poly(lactic-*co*-glycolic acid) (PLGA), have been extensively used to fabricate engineering scaffolds and drug carriers, because of their excellent biocompatibility, biodegradability, and convenient processability.[3,11−13] However, these polyester polymers have low cell adhesion and proliferation due to their hydrophobic surface character.[14,15] Besides, the porous polyester scaffolds demonstrate poor bioactivity and mechanical properties,[12,16] which limit their applications in bone tissue engineering. To overcome the above issues, a promising strategy is the combination of bioactive inorganic nanoparticles as fillers inside the polymer matrix. Among a variety of bioactive inorganic nanoparticles, nanohydroxyapatite (HAp) has received much attention, because it has some special properties, including high biocompatibility, excellent absorbability, good cell adhesiveness, outstanding bioactivity, and strong mechanical properties.[17−19] Recently, nanocomposite (NC) porous bioscaffolds made from HAp and synthetic biodegradable polyester, especially HAp/PLLA and

Received: July 23, 2014
Accepted: September 12, 2014
Published: September 12, 2014

HAp/PLGA, were found to have improved cell viability, bioactivity, and mechanical properties compared to the porous polyester scaffolds.[20−22] However, the interface adhesion strength between HAp nanoparticles and polyester polymer matrix is low, as natural HAp and nonpolar polyester polymers are thermodynamically immiscible, resulting in early failure at the HAp−polymer interface.[8] Surface modification of HAp nanoparticles is a potential strategy to address the above problem. Hong et al. reported that PLLA surface-grafted HAp (g-HAp) nanoparticles could enhance the adhesion strength between the nanoparticles and the polymer matrix.[23,24] And the NC porous scaffolds of g-HAp/PLGA fabricated by the melt-molding particulate leaching method exhibited good biocompatibility, homogeneity, and mechanical properties.[25] Nonetheless, the above report involved relatively complex and time-consuming process for removing the porogens. Therefore, it is imperative to develop a simple and effective method for the preparation of g-HAp/polyesters porous scaffolds.

Recently, Pickering high internal phase emulsion (HIPE) templates have obtained increasing attention to fabricate NC porous scaffolds with well-defined porous structure.[26−30] The fabrication process involves preparing a Pickering HIPE, i.e., a solid particle-stabilized emulsion with the internal phase volume larger than 74%,[31−37] and subsequently solidifying the emulsion external phase. In Pickering HIPEs, solid particles are irreversibly adsorbed at the oil/water interface due to their high attachment energy, which makes the resulting emulsion extremely stable.[38−41] Therefore, Pickering HIPEs are very useful as templates for preparing NC porous scaffolds. As significant progress has been made in the fabrication of NC porous scaffolds from Pickering HIPEs, the polymerization of the monomers in the external phase become the most common method for the solidification of the Pickering HIPEs. The polymerization of the monomers demands additional strict control in the chemical reaction process, which may be challenging.[42] Hence, the facile fabrication of NC porous scaffolds using Pickering HIPE templates that would not involve chemical reactions is highly desirable.

In this work, we reported a simple and effective method to prepare g-HAp/PLGA porous scaffolds by Pickering HIPE templates for bone tissue engineering applications. The schematic illustration is shown in Figure 1. To be specific, we employed g-HAp nanoparticles as particle stabilizers to prepare water-in-dichloromethane (W/O) Pickering HIPEs containing PLGA in oil phase. Then, the NC scaffolds were easily fabricated by evaporating the solvents in the Pickering HIPEs. The effects of g-HAp concentration and internal phase volume fraction on the emulsion morphology, pore structure, and mechanical properties of the NC scaffolds were discussed in detail. Furthermore, the bioactivity, anti-inflammatory drug release behavior, and biocompatibility of NC scaffolds were also investigated.

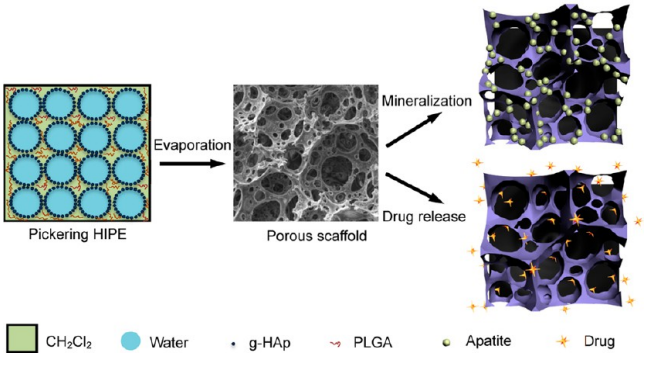

Figure 1. Schematic illustration of fabrication of g-HAp/PLGA NC scaffolds by water-in-CH_2Cl_2 Pickering HIPE templates.

2. EXPERIMENTAL SECTION

2.1. Materials. PLGA (LA/GA = 50:50, weight-average molecular weight M_W = 100 000 g/mol) and PLLA with carboxyl end groups (M_W = 10 000 g/mol) were obtained from Shandong Medical Instrument Research Institute (Jinan, China). HAp nanoparticles were synthesized based on our previous study.[43] Dichloromethane (CH_2Cl_2) was purchased from Guangzhou Chemical Factory (Guangzhou, China). Ibuprofen (IBU) was bought from Dalian Melone Pharmaceutical Co., Ltd. (Dalian, China). All chemicals were used as received without any purification. The water used in all experiments was purified using a Millipore purification apparatus (MA, U.S.A.) with a resistivity higher than 18.0 MΩ·cm.

2.2. Fabrication of g-HAp Nanoparticles. First, the dried HAp nanoparticles were heated from room temperature to 800 °C at a rate of 10 °C min^{-1}, and calcined at 800 °C for 1 h. Afterward, 30 mL of CH_2Cl_2 dispersion of calcined HAp nanoparticles (2.0 g) was stirred while 30 mL of CH_2Cl_2 solution of PLLA with carboxyl end groups (2.0 g) was added, and then CH_2Cl_2 was removed by evaporation at room temperature in a fume hood. The dried mixture was heated at 200 °C for 24 h to obtain g-HAp nanoparticles. For further characterization, g-HAp nanoparticles were centrifugally washed three times with CH_2Cl_2 to remove free PLLA. The g-HAp nanoparticles were used to prepare NC scaffolds without purification after heat treatment.

2.3. Preparation of g-HAp/PLGA NC Scaffolds. The g-HAp/PLGA NC scaffolds were prepared by solvent evaporation from W/O Pickering HIPEs. First, g-HAp nanoparticles were uniformly dispersed into a 7.5 w/v% CH_2Cl_2 solution of PLGA with the aid of ultrasound. Thereafter, Pickering HIPE was prepared by adding water to the oil phase in batches and then hand shaking at every turn. The total volume of Pickering HIPE was kept at 20 mL. Furthermore, the as-prepared Pickering HIPE was transferred into cylindrical molds, and dried in a fume hood at room temperature to remove solvents. Herein, the obtained NC scaffold was named as H_xP-y, which meant that the corresponding Pickering HIPE was fabricated at the g-HAp nanoparticle concentration of x w/v% with respect to the continuous phase and inter phase volume fraction of y v/v%.

2.4. Porosity Measurement. The NC scaffold with a diameter of about 12 mm and thickness of 8 mm was used for porosity determination. The porosity (ε) was estimated on the basis of the apparent density (ρ_S) of NC scaffold and the bulk density (ρ_f) of nonporous NC film. And the ρ_S and ρ_f were obtained by calculating the mass/volume ratio of the corresponding samples. The porosity of the sample was calculated according to the following equation:

$$\varepsilon(\%) = (1 - \rho_S/\rho_f) \times 100 \quad (1)$$

Three specimens were measured for each sample to obtain the average value.

2.5. Mechanical Property Testing. The compression tests of NC scaffolds were performed by a material testing machine (SLBL-1KN, Shimadzu) at 25 °C. The samples used for the tests were about 12 mm in diameter and 8 mm in thickness. The cross-head speed was 1.0 mm/min, and the tests went on until 50% reduction in the height of the specimen. The Young's modulus (E) was defined as the slope of the initial linear region of the stress−strain curve. At least three samples were tested for each scaffold, and the mean value was calculated.

2.6. Biomineralization Study. In vitro biomineralization studies were performed in a 1.5 times simulated body fluid (1.5 × SBF) to evaluate the bioactivity of NC scaffolds. The NC scaffolds with a

diameter of about 12 mm and thickness of 4 mm were incubated in 30 mL 1.5 × SBF at 37 °C without vibration. And the media were replaced with fresh 1.5 × SBF solution every other day. After being incubated for predetermined time intervals, the samples were taken out, washed with water three times, and subsequently dried at room temperature. The mass change of NC scaffolds (W) after incubation in 1.5 × SBF was calculated using the following equation:

$$W(\%) = [(m_t - m_0)/m_0] \times 100 \quad (2)$$

where m_t is the mass of NC scaffolds after incubation in 1.5 × SBF at time t, and m_0 represents the original mass of NC scaffolds without mineralization.

2.7. In Vitro Drug Release. The IBU-loaded NC scaffolds were fabricated as described in 2.3 section except that CH_2Cl_2 solution of PLGA containing 5.0 wt % of IBU with respect to the total mass of g-HAp and PLGA. The drug release studies of IBU-loaded NC scaffolds and free IBU were carried out by measuring the absorbance of IBU at 222 nm using an UV−vis spectrophotometer. The IBU-loaded NC scaffold samples (30 mg, 1.5 mg IBU) were placed into different vials containing 30 mL of phosphate buffer saline (PBS, pH = 7.4). And free IBU (1.5 mg) was put in a dialysis bag (cutoff molecular weight 8000 g/mol) containing 5 mL of PBS, and then immersed in a vial containing 25 mL of PBS. All the samples were incubated in a shaking incubator at a speed of 100 rpm at 37 °C. At predetermined time point, 2 mL of release medium was taken out and equal volume of fresh PBS was replenished. The accumulated release rate of IBU was calculated according to the standard IBU absorbance−concentration calibration curve established from standard PBS solutions of IBU. Each experiment was carried out in triplicate, and the average value was taken.

2.8. Characterization. The microstructure of g-HAp nanoparticles and NC scaffolds were examined by a Zeiss EVO 18 scanning electron microscope (SEM) with an X-ray energy dispersive spectrometer (EDS). Samples were gold coated using a sputter coater and observed at 10 kV acceleration voltage. The g-HAp nanoparticles was also observed using a FEI Tecnai 12 transmission electron microscope (TEM) under accelerating voltage of 200 kV. Thermogravimetry analysis (TGA) was carried out in nitrogen atmosphere with a TG209 thermo-analyzer from 40 to 700 °C at a heating rate of 10 °C/min. The hydrodynamic diameter and polydispersity of g-HAp nanoparticles dispersed in CH_2Cl_2 were measured using a Malvern Zetasizer Nano ZS90. The X-ray diffraction (XRD) test of g-HAp nanoparticles was carried out using an X'pert PRO diffractometer with a Cu Kα radiation source at ambient temperature with a range from 10° to 45°. The Pickering HIPEs were observed using a microscope (Carl Zeiss, German) fitted with a digital camera. Fourier transform infrared spectroscopy (FTIR) of the samples were recorded on a German Vector-33 IR instrument in the range from 4000 to 500 cm^{-1} using a KBr pellet.

2.9. In Vitro Biocompatibility Assay. *2.9.1. Cell Culture.* Mouse bone mesenchymal stem cells (BMSCs), purchased from the American Type Culture Collection (ATCC, Manassas, VA), were cultured in Dulbecco's modified eagle medium (DMEM, Gibco) supplemented with 10% (v/v) fetal bovine serum (FBS, Gibco). BMSCs were incubated in a humidified incubator at 37 °C with 5% CO_2 and the medium was refreshed every 3 days. When BMSCs had grown to confluence, they were harvested using 0.25% trypsin solution. Prior to cell culture, the NC scaffolds were sterilized by soaking in 75% ethanol for 6 h, washed with sterile PBS three times, and exposed to UV light for 4 h. And the NC scaffolds were prewetted in the culture medium for 12 h.

2.9.2. Cell Proliferation. The NC scaffolds with a diameter of 6 mm and thickness of 2 mm were placed into 96-well tissue culture plates (TCPS). 40 μL of BMSCs suspension was seeded at a density of 2 × 10^3 cells/well onto the top of the prewetted scaffolds. The cell-seeded scaffolds were incubated in a humidified incubator at 37 °C with 5% CO_2 for 3 h, and then additional 160 μL of culture medium was added into each well. The culture medium was refreshed every 2 days. At designated time intervals, the culture media were removed and the scaffolds were rinsed with PBS three times. 100 μL 3-(4,5-dimethylthiazol-2-yl)-2,5-diphenyl tetrazolium bromide (MTT) solution (5 mg mL^{-1}) was added to each well. After incubation for 4 h at 37 °C, the upper medium was discarded and the intracellular formazan was dissolved in 150 μL of dimethyl sulfoxide by shaking the plates for 10 min. Thereafter, aliquot of 100 μL was pipetted into the well of 96-well TCPS, and the absorbance was measured using a spectrophotometric microplate reader at 570 nm. The cells cultured directly on TCPS were regarded as a negative control. Experiments were performed in triplicate for each sample and the average value was taken.

2.9.3. Cell Morphology. The scaffolds with a diameter of about 12 mm and thickness of 2 mm were placed in the 24-well TCPS. 200 μL of BMSCs suspension was seeded evenly at a density of 1 × 10^4 cells/well onto the top of the prewetted scaffolds. One mL of culture medium was added into each well after being incubated in a humidified incubator at 37 °C with 5% CO_2 for 3 h. The culture medium was changed every 2 days. At designated time point, the cell-loaded scaffold constructs were washed twice with PBS, fixed with 2.5% glutaraldehyde solution for 4 h at room temperature, and then dehydrated using a series of graded alcohol solutions for 15 min. After drying, the samples were coated with gold and observed by SEM.

3. RESULTS AND DISCUSSION

3.1. Preparation of g-HAp Nanoparticles and Pickering HIPEs. HAp nanoparticles were used as particulate emulsifiers after hydrophobicity modification to stabilize W/O HIPEs. In this work, PLLA molecules with carboxyl end groups were used as the biodegradable and biocompatible modifiers to modify the HAp nanoparticles. PLLA molecules were grafted onto HAp surface by forming calcium carboxylate bonds between carboxyl end groups of PLLA and calcium ions on the HAp surfaces.[44−46] SEM and TEM studies of the dried g-HAp nanoparticles (Figure 2a and Supporting Information (SI) Figure S1) indicated that the g-HAp nanoparticles were irregular shape with broad diameter distribution. Dynamic light scattering study of dilute CH_2Cl_2 dispersion of g-HAp nanoparticles (SI Figure S2a) showed that the mean diameter of g-HAp nanoparticles was about 580 nm. Furthermore, the XRD pattern of g-HAp nanoparticles (SI Figure S2b) demonstrated that the peaks of PLLA at 16.7°, 19°, and 22.4° were coexistent with the peaks of HAp nanoparticles at 26°, 27.8°, 31.2°, and 34.3°, which suggested that PLLA were successfully grafted on the HAp surfaces. And the graft ratio of g-HAp was determined using TGA (Figure 2b). It was seen that the HAp nanoparticles exhibited little mass loss while the g-HAp nanoparticles showed obvious mass loss because of the decomposition of PLLA. The amount of PLLA grafted on the HAp nanoparticle surfaces was about 5.5 wt %.

Herein, g-HAp nanoparticles stabilized HIPEs were prepared in the CH_2Cl_2 solution of PLGA. Drop test showed that the prepared emulsions were the W/O type (see SI Figure S3). And these W/O Pickering HIPEs could be stored for longer than one month, showing excellent stability. As control experiments, the emulsification of CH_2Cl_2 dispersion of g-HAp nanoparticles and water, CH_2Cl_2 dispersion of HAp nanoparticles and water, and CH_2Cl_2 solution of PLGA and water were conducted. The first system succeeded in preparing stable HIPEs, whereas the last two systems failed to form stable emulsions. Hence, it was confirmed that the g-HAp nanoparticles were effective particulate emulsifiers to obtain stable HIPEs.[46]

The Pickering HIPEs were observed by optical microscopy. Figure 3 presents the optical images of Pickering HIPEs with different g-HAp nanoparticle concentrations. The emulsion droplets exhibited well-defined spherical shape. With the

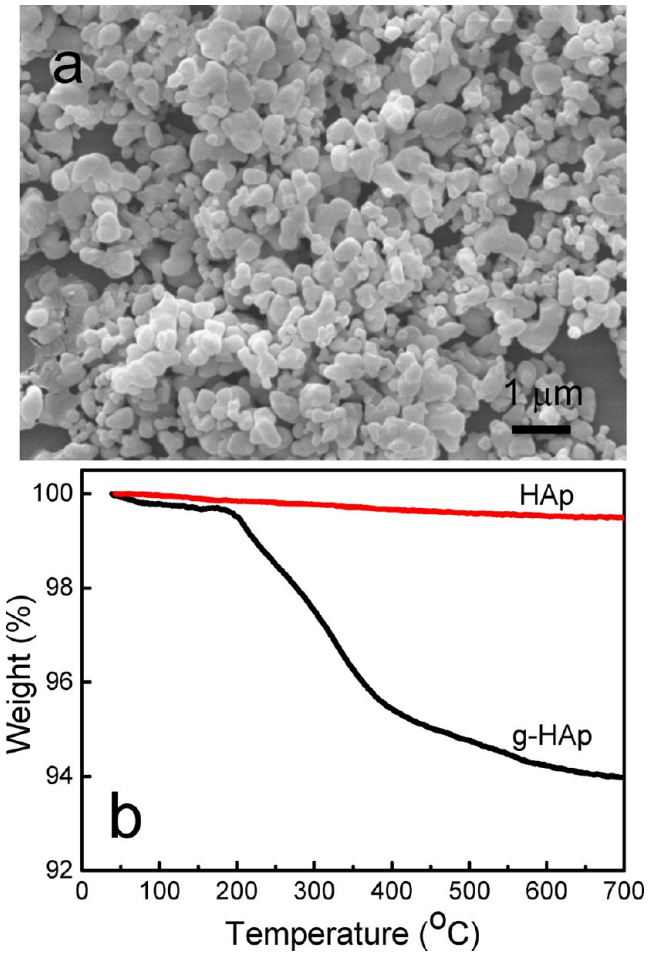

Figure 2. (a) SEM image of g-HAp nanoparticles. (b) TGA curves of HAp nanoparticles and g-HAp nanoparticles.

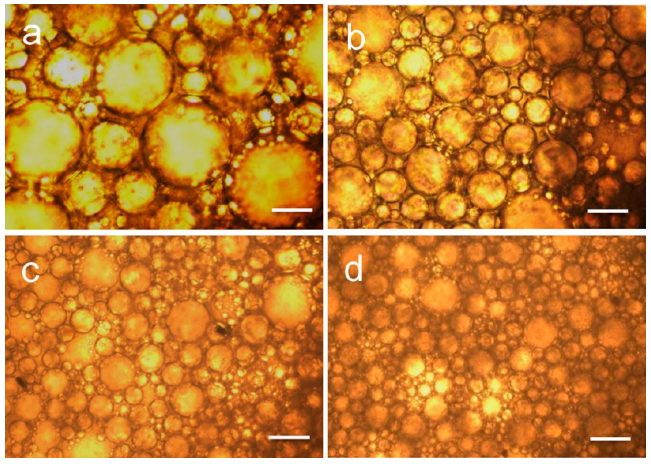

Figure 3. Optical microscopic images of water-in-CH_2Cl_2 Pickering HIPEs prepared with different g-HAp nanoparticle concentrations of: (a) 2.5, (b) 5, (c) 7.5, and (d) 10 w/v%. The scale bars are 60 μm.

increase of g-HAp nanoparticle concentration from 2.5 to 10 w/v%, the emulsion droplet sizes gradually decreased and the emulsion stability was enhanced significantly. This result was attributed to the fact that increased g-HAp nanoparticles could be used to stabilize a larger interfacial area and result in denser nanoparticle layers to enhance the stabilization of the emulsions. Furthermore, the effect of internal phase volume fraction on Pickering HIPEs was also investigated, and the related optical images were shown in SI Figure S4. With increasing internal phase volume fraction from 75 to 90 v/v%, the shape of emulsion droplets changed from well-defined spherical to deformed spherical, and the emulsion droplet sizes increased. The result suggested that with increasing internal phase volume fraction, the fixed concentration of g-HAp nanoparticles became insufficient to cover the increased interfacial areas, leading to the destabilization of Pickering HIPEs.

3.2. Fabrication of NC Scaffolds. The g-HAp/PLGA NC scaffolds were facilely obtained by simple drying of the as-prepared W/O Pickering HIPEs at room temperature. The resulting NC scaffolds were cut by a razor blade after being frozen by liquid nitrogen, and then the cross sections of NC scaffolds were characterized by SEM. The corresponding SEM images are shown in Figures 4,5 and SI Figure S5. As observed,

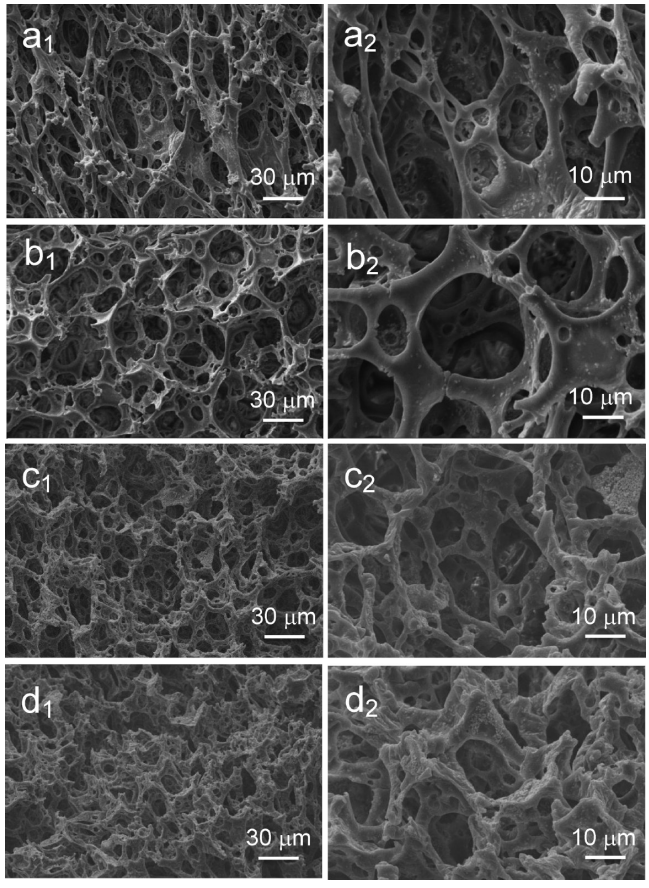

Figure 4. SEM images of NC scaffolds prepared with different g-HAp nanoparticle concentrations of: (a_1 and a_2) 2.5, (b_1 and b_2) 5, (c_1 and c_2) 7.5, and (d_1 and d_2) 10 w/v%.

all NC scaffolds exhibited a highly open-porous structure, and the pores were interconnected by pore throats. Even though the formation of pore throats is a complex process and results from many parameters, it is currently believed that they form in the region of the contact areas of neighboring HIPE droplets.[47] In these areas, the HIPE droplets are separated by only an extremely thin film of the continuous phase, which is unstable in the solvent evaporation process. Furthermore, the pore wall of NC scaffolds was rough because of the g-HAp nanoparticles filled or attached on the pore wall surface. The rough surface of

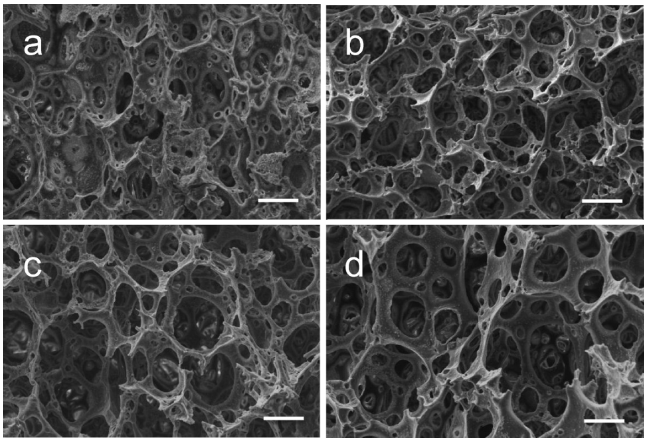

Figure 5. SEM images of NC scaffolds prepared with different internal phase fractions of (a) 75, (b) 80, (c) 85, and (d) 90 vol %. The scale bars are 30 μm.

pore wall was beneficial to improve attachment, proliferation, and differentiation of anchorage-dependent bone forming cells.[25]

Figure 4 presents the SEM images of NC scaffolds prepared at different g-HAp nanoparticle concentrations and internal phase volume fraction of 80%. It was observed that with increasing the g-HAp nanoparticle concentration, the pore shape changed from irregular ellipsoidal to uniform spherical. The pore size and pore throat size decreased gradually. This was because more g-HAp nanoparticles were used to stabilize the emulsions, which enhanced the stabilization of the emulsions and reduced the emulsion droplet sizes, and hence decreased the pore size and pore throat size of NC scaffolds. As the same reason, the apparent density of the NC scaffolds increased and the porosity decreased (Table 1) with the increase of g-HAp nanoparticle concentration. The materials by the HIPE templates of the same internal phase volume should have the same pore volume. However, with the increase of g-HAp concentration, the solid volume of the materials increases, which will decrease the porosity. As expected, increasing the g-HAp nanoparticle concentration resulted in more g-HAp nanoparticles appeared on the surface of pore wall, which enhanced the surface roughness of pore wall.

Table 1. Physical Properties of NC Scaffolds from Pickering HIPEs

samples	absolute density (g cm^{-3})	apparent density (g cm^{-3})	porosity (%)	Young's modulus (MPa)	compressive stress at 40% strain (MPa)
$H_{2.5}$P-80	1.470	0.195	86.7	2.4	0.20
H_5P-80	1.608	0.230	85.7	9.5	0.59
$H_{7.5}$P-80	1.698	0.338	80.1	14.9	0.96
H_{10}P-80	1.766	0.396	77.6	19.2	1.48
H_5P-75	1.608	0.314	80.5	10.1	1.27
H_5P-85	1.608	0.164	89.8	5.5	0.50
H_5P-90	1.608	0.109	93.2	3.4	0.42

SEM images of NC scaffolds prepared at different internal phase volume fractions and g-HAp nanoparticle concentration of 5 w/v% are shown in Figure 5 and SI Figure S4. With increasing internal phase volume fraction, the pore size and pore throat size increased, respectively. The result should be assigned to the reason that the g-HAp nanoparticle concentration available to adsorb at w/o interface became insufficient with increasing the internal phase volume fraction, which resulted in the destabilization of Pickering HIPEs and the formation of bigger emulsion droplets, hence increased the pore size and pore throat size of NC scaffolds. The absolute density of the four NC scaffolds was identical, because the composition in the continuous phase of HIPE templates kept the same. As expected, the apparent density of NC scaffolds decreased and the porosity increased with increasing internal phase volume fraction of the emulsion template (Table 1).

NC scaffolds with different pore structures could be easily fabricated by adjusting the g-HAp nanoparticle concentration or internal phase volume fraction. And the average pore size of NC scaffolds was smaller than the corresponding precursor emulsion droplet size, which might be because the high capillary stresses developed in the drying process resulted in the volume shrinkage from precursor HIPE to the corresponding scaffold. Nevertheless, the interconnected macroporous NC scaffolds with the pore sizes ranging from a few microns to several tens of microns were successfully prepared. Therefore, the g-HAp nanoparticle stabilized HIPEs used as initial templates were extremely effective to form hierarchical macroporous NC scaffolds. Additionally, the NC scaffolds were examined by EDS to assess the compositions and their distribution on the pore wall surface. EDS results of scaffold H_5P-80 showed that the main elements were carbon (C), oxygen (O), calcium (Ca), and phosphorus (P) (SI Figure S6). As is well known, the elements Ca and P were derived from g-HAp nanoparticles. The elements Ca and P were uniformly distributed on the pore wall surface, which suggested that g-HAp nanoparticles were evenly embedded in the pore wall of NC scaffolds. Noting that the Ca/P molar ratio was 1.68, which was similar to the Ca/P molar ratio of 1.67 in HAp from natural bone.

3.3. Mechanical Property of NC Scaffolds. Mechanical property is an important indice in the preparation of porous scaffolds to arrive the requirements for the bone tissue engineering application. Thus, compression tests were conducted to evaluate the mechanical properties of the NC scaffolds prepared varying g-HAp nanoparticle concentration and internal phase volume fraction. The Young's modulus and compressive stress at 40% strain of NC scaffolds are summarized in Table 1. It was observed that with increasing g-HAp nanoparticle concentration, the Young's modulus and compressive stress at 40% strain significantly increased. The result was likely attributed to the fact that the rigid g-HAp nanoparticles could enhance stress transfer from the polymer matrix to the g-HAp nanoparticles. Therefore, the higher concentration of g-HAp nanoparticles, the more efficient stress transfers from the polymer matrix to the g-HAp nanoparticles, which greatly improved the compressive modulus and stress. However, increasing the g-HAp nanoparticle concentration visibly decreased the porosity of NC scaffolds, which could be another major reason to the improved the compressive modulus and stress. Furthermore, it was also seen that the internal phase volume fraction affected the mechanical properties of NC scaffolds. With the increase in the internal phase volume fraction, both the compressive modulus and stress gradually decreased, which were consistent with the previous literature.[48] This was probably ascribed to the fact that increasing the internal phase volume fraction obviously increased the porosity of NC scaffolds, which led to a significant reduction of compressive modulus and stress of

NC scaffolds. In short, the above results indicated that the mechanical properties of NC scaffolds could be controlled by adjusting g-HAp nanoparticle concentration or internal phase volume fraction.

3.4. Biomineralization on NC Scaffolds. The in vitro biomineralization studies were performed to testify the bioactivity of NC scaffolds. Herein, the NC scaffolds prepared with varying g-HAp nanoparticle concentrations were immersed in 1.5 × SBF at 37 °C up to 14 days. Figure 6a shows the mass changes of NC scaffolds after mineralization for various time periods. It was observed that all NC scaffolds showed a remarkable mass increase with the prolongation of the incubation time. According to the literature,[9] the mass changes of the degradable polymer-based scaffolds after mineralization in SBF were ascribed to the two competing processes of scaffold degradation and apatite deposition. Hence, the obvious mass increase of the mineralized NC scaffolds showed that the deposition rates of apatite were greatly higher than the loss rates of the NC scaffolds due to their degradation. Furthermore, it was also seen that the mass increase rate of NC scaffolds enhanced with increasing g-HAp nanoparticle concentration for the same incubation time. This might be ascribed to the fact that the g-HAp nanoparticle surfaces contained a great many hydroxyl groups, which might ionize in 1.5 × SBF (pH 7.4) to form negatively charged units because of the isoelectric point of HAp nanoparticles of around pH 6. And the g-HAp nanoparticles with negative charges on their surfaces could act as initial nucleation sites, which attracted the positive calcium ions from the 1.5 × SBF, and in turn interacted with the negative phosphate ions leading to the formation of bonelike apatite. Hence, the higher concentration of g-HAp nanoparticles used to prepare NC scaffolds, the more nucleation initiation sites and negative charges existed, consequently the more apatite would deposit on the NC scaffolds. The above results suggested that the addition of g-HAp nanoparticles enhanced the bioactivity of polymer scaffolds.

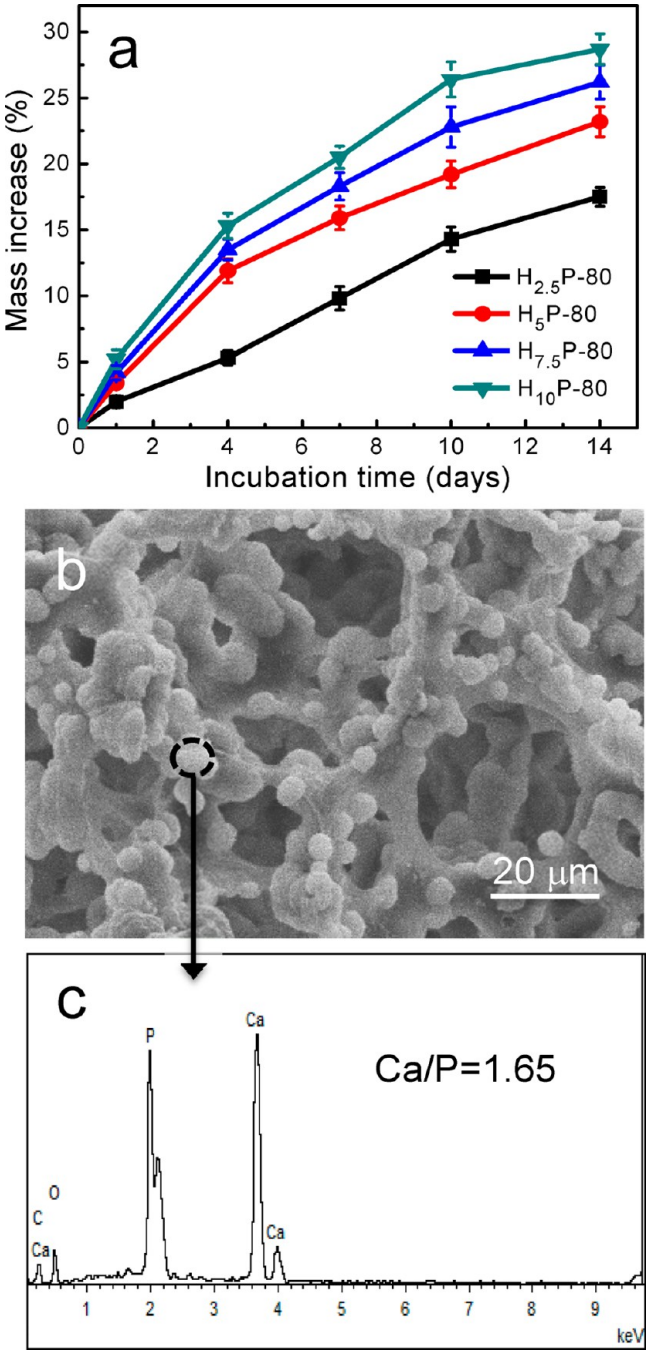

Figure 6. (a) Mass increase vs incubation time in 1.5 × SBF for NC scaffolds prepared at different g-HAp nanoparticle concentration. Error bars indicate SD (n = 3). SEM image (b) showing morphology of the mineral formed on scaffold H_5P-80 after 4 days incubation in 1.5 × SBF. EDS spectrum (c) shows the mineral composition on the area reported in (b).

To understand the morphology of the apatite deposited on the NC scaffolds, the mineralized NC scaffolds were observed by SEM. An example was reported in Figure 6b, which referred to the scaffold H_5P-80 immersed in 1.5 × SBF after 4 days. Figure 6b revealed that the scattered spherical apatite particles were deposited randomly on the pore wall surface of NC scaffold. And the average size of apatite particles was about 4.3 μm. Furthermore, the composition of the apatite particles was further discussed by EDS (Figure 6c). The result of EDS spectrum showed the major elements of apatite consisted of carbon (C), oxygen (O), phosphorus (P), and calcium (Ca). And the Ca/P molar ratio of apatite was 1.65, which was slightly less than that of pure HAp (1.67), indicating the presence of calcium-sufficient apatite on the pore wall surface of NC scaffold. It might be attributed to the substitution at PO_4^{3-} sites by HPO_4^{2-}.

3.5. In Vitro Anti-inflammatory Drug Release Study. In this work, we have chosen IBU as the model drug, because it is a potent anti-inflammatory drug which has been widely used in tissue engineering to mitigate immune response. Herein, IBU was dissolved into CH_2Cl_2 solution of PLGA to prepare IBU-loaded NC scaffolds by solvent evaporation from Pickering HIPEs. SI Figure S7 shows the FTIR spectra of scaffold H_5P-80 before and after loading of IBU. In the spectrum of IBU-loaded scaffold H_5P-80, the peak at 1721 cm^{-1}, which originated from the typical stretching vibration of carboxyl groups in IBU, could be observed, indicating the successful loading of IBU in the NC scaffold. And the SEM image of IBU-loaded scaffold H_5P-80 (SI Figure S8) showed that the pore structure of IBU-loaded NC scaffold was similar to that of NC scaffold without IBU (Figure 5b), which suggested that IBU was little influence for the pore structure of the NC scaffolds. Furthermore, the drug loading efficiencies of the IBU-loaded scaffolds were determined by the extraction method reported in our previous work.[49] The drug loading efficiencies of IBU-loaded scaffolds

fabricated at 2.5, 5, 7.5, and 10 w/v% of g-HAp nanoparticle concentrations were 97.2%, 98.6%, 99.1%, 99.4%, respectively. Hence, solvent evaporation from Pickering HIPE templates was a facile and effective method to form drug-loaded porous scaffolds.

Figure 7 shows the in vitro release profiles of IBU in PBS from NC scaffolds prepared with different g-HAp nanoparticle

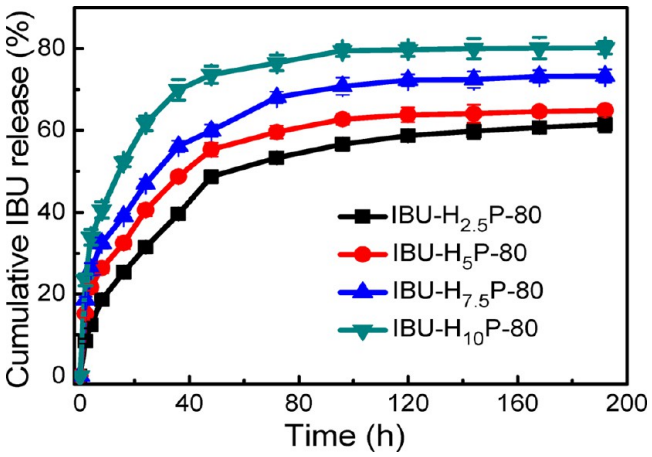

Figure 7. In vitro release profiles of IBU from IBU-loaded scaffolds incubated in PBS at 37 °C.

concentrations. It could be seen that all samples showed the similar IBU release profiles during the study period, which consisted of an initial fast release phase (burst release) and then a successive sustained release phase. For instance, the released amounts of IBU from IBU-loaded scaffold H_5P-80 were about 55.3% in 48 h and about 64.9% in 192 h, respectively. The initial fast release stage should be ascribed to the rapid release of IBU from the outer surfaces and pore entrances. After 48 h, the release profile of IBU became relatively slow, which should be attributed to the increase in diffusion path length of IBU and the interaction between the carboxyl groups of IBU and the hydroxyl groups from the surfaces of g-HAp nanoparticles. In addition, the release rate and maximum amount of IBU released from the NC scaffolds increased with the increase in g-HAp nanoparticle concentration, despite the decrease in porosity of NC scaffolds. This might be mainly attributed to the hydrophilicity of g-HAp nanoparticles, which was beneficial for release medium penetrating into the NC scaffolds, and in turn facilitated the dissolving process of IBU into the release medium. Hence, the higher drug release was observed from the release profile of NC scaffolds prepared at higher g-HAp nanoparticle concentration. For comparison, the release kinetics of free IBU was also investigated in PBS at 37 °C, and the result is shown in SI Figure S9. It was clearly seen that the release of free IBU was very fast, and approximate 92.2% IBU was released within 1 h. Considering the controlled IBU release profile of NC scaffolds, the long-term anti-inflammatory effect can be anticipated, when they are applied as drug loaded engineered scaffolds for bone repair and regeneration.

3.6. Proliferation and Morphology of BMSCs on NC Scaffolds. Cell proliferation is an important initial parameter to evaluate the biocompatibility of scaffolds for tissue engineering application. Herein, we cultured BMSCs on TCPS and NC scaffolds prepared with different g-HAp nanoparticle concentrations, and determined cell proliferation ability using MTT assay after being cultured for 1, 4, and 7 days. As shown in Figure 8, the cell viability of BMSCs on both TCPS and NC scaffolds increased significantly with increasing

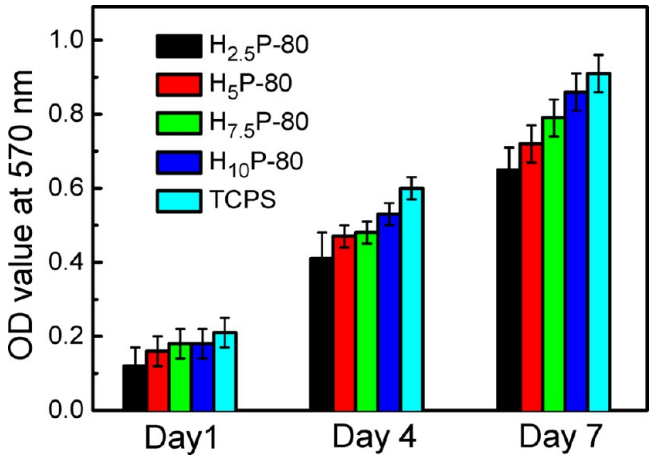

Figure 8. Cell viability of BMSCs after 1, 4, and 7 days of culture on NC scaffolds and TCPS as a function of time, measured by MTT assay.

culturing time. Furthermore, it was also seen that the NC scaffolds with relatively high g-HAp nanoparticle concentration exhibited an obviously increased optical density (OD) value, indicating that the g-HAp nanoparticles facilitated cell growth and further promoted cell proliferation. The result was likely to be associated with the chemical composition and the surface topography of the NC scaffolds. The incorporation of g-HAp nanoparticles into the polymer matrix lead to a change in the chemical composition of NC scaffolds. To be specific, increasing the g-HAp nanoparticle concentration in the NC scaffolds enhances the amount of HAp, because HAp is the main composite in g-HAp. The introduction of HAp in scaffolds is beneficial for the improvement of cell viability.[50] In addition, with the increase in the g-HAp nanoparticle concentration, the surface roughness of NC scaffolds is enhanced, which is active in facilitating cell adhesion and proliferation.[51] Overall, although cell viability on NC scaffolds was lower than that on TCPS, the experiments demonstrated the ability of NC scaffolds to support cell growth and promoted cell proliferation, and consequently give an indication of the biocompatibility of g-HAp/PLGA NC scaffolds.

To further examine the biocompatibility of NC scaffolds, we evaluated the distribution and morphology of BMSCs cultured on scaffold H_5P-80 using SEM. It was found that after 4 days of cell seeding, most of the BMSCs attached and grew on the scaffold surfaces, while a few BMSCs could be found in the inner pores of the scaffolds (SI Figure S10). Furthermore, representative SEM images of BMSCs cultured on scaffold H_5P-80 after different culture time are shown in Figure 9. After 1 day of cell seeding, the morphology of BMSCs was largely in flattened round shape. After 4 days of cell seeding, the cells were bipolar extensions and showed a spindle shape with elongated pseudopodia. More interestingly, after 7 days of cell seeding, the cells formed a confluent layer, indicating the good cell viability of NC scaffolds. Combined with the results from MTT, we concluded that the NC scaffolds had good biocompatibility with BMSCs and were potential engineering scaffolds for biomedical applications.

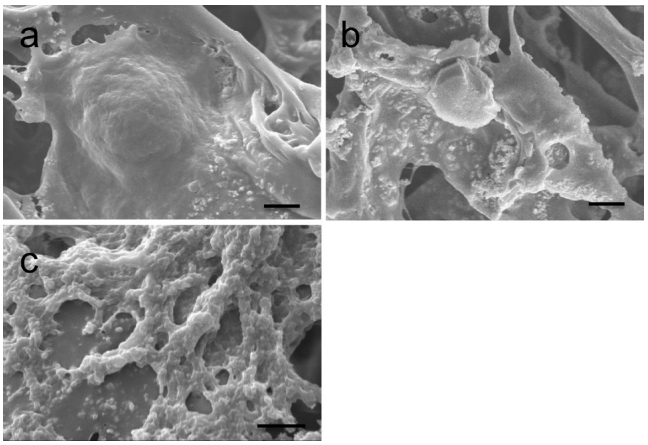

Figure 9. SEM images of BMSCs seeded on scaffold H_5P-80 after (a) 1 day, (b) 4 days, and (c) 7 days culture. The scale bars are 5 μm.

4. CONCLUSIONS

g-HAp/PLGA NC porous scaffolds with rough pore wall surfaces were facilely prepared by solvent evaporation from templating g-HAp nanoparticle-stabilized W/O Pickering HIPEs. The emulsion morphology, pore structure, and mechanical properties of the scaffolds could be tailored by varying the g-HAp nanoparticle concentration or internal phase volume fraction of the emulsion template. The emulsion size, pore size, and porosity decreased, while the compressive modulus and compressive stress at 40% stain enhanced with increasing g-HAp nanoparticle concentration or decreasing internal phase volume fraction. The NC scaffolds with varying g-HAp nanoparticle concentrations were used as matrixes for the mineralization study in SBF. The results showed that the mass of apatite particles formed on the NC scaffolds increased with the increase in incubation time and the concentration of g-HAp nanoparticles. And the apatite particles were similar to the apatite in natural bone. The anti-inflammatory drug IBU was easily loaded into the NC scaffolds by dispersing it in the oil phase in the fabrication process. The drug release studies indicated that the IBU-loaded scaffolds displayed a sustained release profile, and the release rate increased with higher g-HAp nanoparticle concentration. Cell culture assay results showed the NC scaffolds supported adhesion, spread and proliferation of BMSCs, showing the biocompatibility of NC scaffolds. Overall, the above results demonstrated the feasibility of NC scaffolds templated from Pickering HIPEs as promising biodegradable and bioactive biomaterials for bone tissue engineering applications.

■ ASSOCIATED CONTENT

Ⓢ Supporting Information

Characterization of g-HAp nanoparticles, Pickering HIPEs, and NC scaffolds. This material is available free of charge via the Internet at http://pubs.acs.org.

■ AUTHOR INFORMATION

Corresponding Author

*Tel/Fax: +86-20-22236269; e-mail: zhywang@scut.edu.cn.

Notes

The authors declare no competing financial interest.

■ ACKNOWLEDGMENTS

This work was financially supported by the National Natural Basic Research Program of China (973 Program, 2012CB821500), the National Natural Science Foundation of China (21274046 and 21474032), and the Natural Science Foundation of Guangdong Province (S2012020011057).

■ REFERENCES

(1) Liu, H. H.; Peng, H. J.; Wu, Y.; Zhang, C.; Cai, Y. Z.; Xu, G. W.; Li, Q.; Chen, X.; Ji, J. F.; Zhang, Y. Z.; OuYang, H. W. The Promotion of Bone Regeneration by Nanofibrous Hydroxyapatite/Chitosan Scaffolds by Effects on Integrin-BMP/Smad Signaling Pathway in BMSCs. *Biomaterials* **2013**, *34*, 4404−4417.

(2) Dash, M.; Samal, S. K.; Bartoli, C.; Morelli, A.; Smet, P. F.; Dubruel, P.; Chiellini, F. Biofunctionalization of Ulvan Scaffolds for Bone Tissue Engineering. *ACS Appl. Mater. Interfaces* **2014**, *6*, 3211−3218.

(3) Reverchon, E.; Pisanti, P.; Cardea, S. Nanostructured PLLA-Hydroxyapatite Scaffolds Produced by a Supercritical Assisted Technique. *Ind. Eng. Chem. Res.* **2009**, *48*, 5310−5316.

(4) Liu, X. H.; Smith, L. A.; Hu, J.; Ma, P. X. Biomimetic Nanofibrous Gelatin/Apatite Composite Scaffolds for Bone Tissue Engineering. *Biomaterials* **2009**, *30*, 2252−2258.

(5) Persson, M.; Lorite, G. S.; Cho, S. W.; Tuukkanen, J.; Skrifvars, M. Melt Spinning of Poly(lactic acid) and Hydroxyapatite Composite Fibers: Influence of the Filler Content on the Fiber Properties. *ACS Appl. Mater. Interfaces* **2013**, *5*, 6864−6872.

(6) He, C. L.; Jin, X. B.; Ma, P. X. Calcium Phosphate Deposition Rate, Structure and Osteoconductivity on Electrospun Poly(L-lactic acid) Matrix using Electrodeposition or Simulated Body Fluid Incubation. *Acta Biomater.* **2014**, *10*, 419−427.

(7) Fu, Q.; Saiz, E.; Rahaman, M. N.; Tomsia, A. P. Toward Strong and Tough Glass and Ceramic Scaffolds for Bone Repair. *Adv. Funct. Mater.* **2013**, *23*, 5461−5476.

(8) Zhang, P. B.; Hong, Z. K.; Yu, T.; Chen, X. S.; Jing, X. B. In Vivo Mineralization and Osteogenesis of Nanocomposite Scaffold of Poly(lactide-*co*-glycolide) and Hydroxyapatite Surface-grafted with Poly(L-lactide). *Biomaterials* **2009**, *30*, 58−70.

(9) Zhu, M.; Zhang, L. X.; He, Q. J.; Zhao, J. J.; Limin, G.; Shi, J. L. Mesoporous Bioactive Glass-Coated Poly(L-lactic acid) Scaffolds: a Sustained Antibiotic Drug Release System for Bone Repairing. *J. Mater. Chem.* **2011**, *21*, 1064−1072.

(10) Baradari, H.; Damia, C.; Dutreih-Colas, M.; Laborde, E.; Pécout, N.; Champion, E.; Chulia, D.; Viana, M. Calcium Phosphate Porous Pellets as Drug Delivery Systems: Effect of Drug Carrier Composition on Drug Loading and In Vitro Release. *J. Eur. Ceram. Soc.* **2012**, *32*, 2679−2690.

(11) Shi, X. T.; Zhao, Y. H.; Zhou, J. H.; Chen, S.; Wu, H. K. One-Step Generation of Engineered Drug-Laden Poly(lactic-*co*-glycolic acid) Micropatterned with Teflon Chips for Potential Application in Tendon Restoration. *ACS Appl. Mater. Interfaces* **2013**, *5*, 10583−10590.

(12) Zhang, Q. W.; Mochalin, V. N.; Neitzel, I.; Hazeli, K.; Niu, J. J.; Kontsos, A.; Zhou, J. G.; Lelkes, P. I.; Gogotsi, Y. Mechanical Properties and Biomineralization of Multifunctional Nanodiamond-PLLA Composites for Bone Tissue Engineering. *Biomaterials* **2012**, *33*, 5067−5075.

(13) Zhou, C. J.; Shi, Q. F.; Guo, W. H.; Terrell, L.; Qureshi, A. T.; Hayes, D. J.; Wu, Q. L. Electrospun Bio-Nanocomposite Scaffolds for Bone Tissue Engineering by Cellulose Nanocrystals Reinforcing Maleic Anhydride Grafted PLA. *ACS Appl. Mater. Interfaces* **2013**, *5*, 3847−3854.

(14) Shen, H.; Hu, X. X.; Yang, F.; Bei, J. Z.; Wang, S. G. Cell Affinity for bFGF Immobilized Heparin-Containing Poly(lactide-*co*-glycolide) Scaffolds. *Biomaterials* **2011**, *32*, 3404−3412.

(15) Liu, X. W.; Okada, M.; Maeda, H.; Fujii, S.; Furuzono, T. Hydroxyapatite/Biodegradable Poly(L-lactide-*co*-caprolactone) Com-

posite Microparticles as Injectable Scaffolds by a Pickering Emulsion Route. *Acta Biomater.* **2011**, *7*, 821−828.
(16) Kum, C. H.; Cho, Y.; Joung, Y. K.; Choi, J.; Park, K.; Seo, S. H.; Park, Y. S.; Ahn, D. J.; Han, D. K. Biodegradable Poly(L-lactide) Composites by Oligolactide-Grafted Magnesium Hydroxide for Mechanical Reinforcement and Reduced Inflammation. *J. Mater. Chem. B* **2013**, *1*, 2764−2772.
(17) Zhou, S. S.; Bismarck, A.; Steinke, J. H. G. Interconnected Macroporous Glycidyl Methacrylate-Grafted Dextran Hydrogels Synthesised from Hydroxyapatite Nanoparticle Stabilised High Internal Phase Emulsion Templates. *J. Mater. Chem.* **2012**, *22*, 18824−18829.
(18) Jia, L. P.; Duan, Z. G.; Fan, D. D.; Mi, Y.; Hui, J. F.; Chang, L. Human-like Collagen/ Nano-Hydroxyapatite Scaffolds for the Culture of Chondrocytes. *Mater. Sci. Eng., C* **2013**, *33*, 727−734.
(19) Fujii, S.; Okada, M.; Sawa, H.; Furuzono, T.; Nakamura, Y. Hydroxyapatite Nanoparticles as Particulate Emulsifier: Fabrication of Hydroxyapatite-Coated Biodegradable Microspheres. *Langmuir* **2009**, *25*, 9759−9766.
(20) Peng, F.; Yu, X. H.; Wei, M. In Vitro Cell Performance on Hydroxyapatite Particles/Poly(L-lactic acid) Nanofibrous Scaffolds with an Excellent Particle along Nanofiber Orientation. *Acta Biomater.* **2011**, *7*, 2585−2592.
(21) Li, M. M.; Liu, W. W.; Sun, J. S.; Xianyu, Y. L.; Wang, J. D.; Zhang, W.; Zheng, W. F.; Huang, D. Y.; Di, S. Y.; Long, Y. Z.; Jiang, X. Y. Culturing Primary Human Osteoblasts on Electrospun Poly(lactic-*co*-glycolic acid) and Poly(lactic-*co*-glycolic acid)/Nanohydroxyapatite Scaffolds for Bone Tissue Engineering. *ACS Appl. Mater. Interfaces* **2013**, *5*, 5921−5926.
(22) Zheng, F. Y.; Wang, S. G.; Wen, S. H.; Shen, M. W.; Zhu, M. F.; Shi, X. G. Characterization and Antibacterial Activity of Amoxicillin-Loaded Electrospun Nano-Hydroxyapatite/ Poly(lactic-*co*-glycolic acid) Composite Nanofibers. *Biomaterials* **2013**, *34*, 1402−1412.
(23) Hong, Z. K.; Zhang, P. B.; He, C. L.; Qiu, X. Y.; Liu, A. X.; Chen, L.; Chen, X. S.; Jing, X. B. Nano-Composite of Poly(L-lactide) and Surface Grafted Hydroxyapatite: Mechanical Properties and Biocompatibility. *Biomaterials* **2005**, *26*, 6296−6304.
(24) Hong, Z. K.; Zhang, P. B.; Liu, A. X.; Chen, L.; Chen, X. S.; Jing, X. B. Composites of Poly(lactide-*co*-glycolide) and the Surface Modified Carbonated Hydroxyapatite Nanoparticles. *J. Biomed. Mater. Res. A* **2007**, *81*, 515−522.
(25) Cui, Y.; Liu, Y.; Cui, Y.; Jing, X. B.; Zhang, P. B.; Chen, X. S. The Nanocomposite Scaffold of Poly(lactide-*co*-glycolide) and Hydroxyapatite Surface-Grafted with L-lactic Acid Oigomer for Bone Repair. *Acta Biomater.* **2009**, *5*, 2680−2692.
(26) Ikem, V. O.; Menner, A.; Horozov, T. S.; Bismarck, A. Highly Permeable Macroporous Polymers Synthesized from Pickering Medium and High Internal Phase Emulsion Templates. *Adv. Mater.* **2010**, *22*, 3588−3592.
(27) Zheng, Z.; Zheng, X. H.; Wang, H. T.; Du, Q. G. Macroporous Graphene Oxide-Polymer Composite Prepared through Pickering High Internal Phase Emulsions. *ACS Appl. Mater. Interfaces* **2013**, *5*, 7974−7982.
(28) Zou, S. W.; Wei, Z. J.; Hu, Y.; Deng, Y. H.; Tong, Z.; Wang, C. Y. Macroporous Antibacterial Hydrogels with Tunable Pore Structures Fabricated by Using Pickering High Internal Phase Emulsions as Templates. *Polym. Chem.* **2014**, *5*, 4227−4234.
(29) Vílchez, A.; Rodríguez-Abreu, C.; Esquena, J.; Menner, A.; Bismarck, A. Macroporous Polymers Obtained in Highly Concentrated Emulsions Stabilized Solely with Magnetic Nanoparticles. *Langmuir* **2011**, *27*, 13342−13352.
(30) Menner, A.; Ikem, V.; Salgueiro, M.; Shaffer, M. S. P.; Bismarck, A. High Internal Phase Emulsion Templates Solely Stabilised by Functionalised Titania Nanoparticles. *Chem. Commun.* **2007**, 4274−4276.
(31) Li, Z. F.; Ngai, T. Macroporous Polymer from Core-Shell Particle-Stabilized Pickering Emulsions. *Langmuir* **2010**, *26*, 5088−5092.
(32) Destribats, M.; Faure, B.; Birot, M.; Babot, O.; Schmitt, V.; Backov, R. Tailored Silica Macrocellular Foams: Combining Limited Coalescence-Based Pickering Emulsion and Sol-Gel Process. *Adv. Funct. Mater.* **2012**, *22*, 2642−2654.
(33) Cai, D. Y.; Thijssen, J. H. T.; Clegg, P. S. Making Non-aqueous High Internal Phase Pickering Emulsions: Influence of Added Polymer and Selective Drying. *ACS Appl. Mater. Interfaces* **2014**, *6*, 9214−9219.
(34) Colver, P. J.; Bon, S. A. F. Cellular Polymer Monoliths Made via Pickering High Internal Phase Emulsions. *Chem. Mater.* **2007**, *19*, 1537−1539.
(35) Li, Z. F.; Xiao, M. D.; Wang, J. F.; Ngai, T. Pure Protein Scaffolds from Pickering High Internal Phase Emulsion Template. *Macromol. Rapid Commun.* **2013**, *34*, 169−174.
(36) Chen, Y. H.; Ballard, N.; Bon, S. A. F. Moldable High Internal Phase Emulsion Hydrogel Objects from Non-covalently Crosslinked Poly(*N*-isopropylacrylamide) Nanogel Dispersions. *Chem. Commun.* **2013**, *49*, 1524−1526.
(37) Yang, Y.; Tong, Z.; Ngai, T.; Wang, C. Y. Nitrogen-Rich and Fire-Resistant Carbon Aerogels for the Removal of Oil Contaminants from Water. *ACS Appl. Mater. Interfaces* **2014**, *6*, 6351−6360.
(38) Hermes, M.; Clegg, P. S. Yielding and Flow of Concentrated Pickering Emulsions. *Soft Matter* **2013**, *9*, 7568−7575.
(39) Colver, P. J.; Bon, S. A. F. Cellular Polymer Monoliths Made via Pickering High Internal Phase Emulsions. *Chem. Mater.* **2007**, *19*, 1537−1539.
(40) Zhao, Y. L.; Yin, G. N.; Zheng, Z.; Wang, H. T.; Du, Q. G. Preparation of Polymer Hollow Microspheres Covered by Polymer Solid Particles via Two Polymerization Steps. *J. Polym. Sci., Part A: Polym. Chem.* **2011**, *49*, 5257−5269.
(41) Zang, D. Y.; Clegg, P. S. Relationship between High Internal-Phase Pickering Emulsions and Catastrophic Inversion. *Soft Matter* **2013**, *9*, 7042−7048.
(42) Li, Z. F.; Ming, T.; Wang, J. F.; Ngai, T. High Internal Phase Emulsions Stabilized Solely by Microgel Particles. *Angew. Chem., Int. Ed.* **2009**, *48*, 8490−8493.
(43) Hu, Y.; Yang, Y.; Ning, Y.; Wang, C. Y.; Tong, Z. Facile Preparation of Artemisia Argyi Oil-Loaded Antibacterial Microcapsules by Hydroxyapatite-Stabilized Pickering Emulsion Templating. *Colloids Surf., B* **2013**, *112*, 96−102.
(44) Qiu, X. Y.; Chen, L.; Hu, J. L.; Sun, J. R.; Hong, Z. K.; Liu, A. X.; Chen, X. S.; Jing, X. B. Surface-Modified Hydroxyapatite Linked by L-Lactic Acid Oligomer in the Absence of Catalyst. *J. Polym. Sci., Part A: Polym. Chem.* **2005**, *43*, 5177−5185.
(45) Hu, Y.; Gu, X. Y.; Chen, W. K.; Zou, S. W.; Wang, C. Y. Macroporous Nanocomposite Materials Prepared by Solvent Evaporation from Pickering Emulsion Templates. *Macromol. Mater. Eng.* **2014**, *299*, 1070−1080.
(46) Maeda, H.; Okada, M.; Fujii, S.; Nakamura, Y.; Furuzono, T. Pickering-Type Water-in-Oil-in-Water Multiple Emulsions toward Multihollow Nanocomposite Microspheres. *Langmuir* **2010**, *26*, 13727−13731.
(47) Manley, S. S.; Graeber, N.; Grof, Z.; Menner, A.; Hewitt, G. F.; Stepanek, F.; Bismarck, A. New Insights into the Relationship between Internal Phase Level of Emulsion Templates and Gas-Liquid Permeability of Interconnected Macroporous Polymers. *Soft Matter* **2009**, *5*, 4780−4787.
(48) Li, T. T.; Liu, H. R.; Zeng, L.; Yang, S.; Li, Z. C.; Zhang, J. D.; Zhou, X. T. Macroporous Magnetic Poly(styrene−divinylbenzene) Nanocomposites Prepared via Magnetite Nanoparticles- Stabilized High Internal Phase Emulsions. *J. Mater. Chem.* **2011**, *21*, 12865−12872.
(49) Hu, Y.; Zou, S. W.; Chen, W. K.; Tong, Z.; Wang, C. Y. Mineralization and Drug Release of Hydroxyapatite/Poly(L-lactic acid) Nanocomposite Scaffolds Prepared by Pickering Emulsion Templating. *Colloids Surf., B* **2014**, DOI: 10.1016/j.colsurfb.2014.07.032.
(50) Jiang, H.; Zuo, Y.; Zou, Q.; Wang, H. N.; Du, J. J.; Li, Y. B.; Yang, X. C. Biomimetic Spiral-Cylindrical Scaffold Based on Hybrid Chitosan/Cellulose/Nano-Hydroxyapatite Membrane for Bone Regeneration. *ACS Appl. Mater. Interfaces* **2013**, *5*, 12036−12044.

(51) Cheng, D. L.; Cao, X. D.; Gao, H. C.; Wang, Y. J. Engineering Poly(lactic-*co*-glycolic acid)/Calcium Carbonate Microspheres with Controllable Topography and Their Cell Response. *J. Mater. Chem. B* **2013**, *1*, 3322−3329.